ADVANCED MATERIALS
www.advmat.de

Nanostructured, Fluid-Bicontinuous Gels for Continuous-Flow Liquid–Liquid Extraction

*Mohd A. Khan, Alessio J. Sprockel, Katherine A. Macmillan, Meyer T. Alting, Shankar P. Kharal, Stephen Boakye-Ansah, and Martin F. Haase**

Fluid-bicontinuous gels are unique materials that allow two distinct fluids to interact through a percolating, rigid scaffold. Current restrictions for their use are the large fluid-channel sizes (>5 µm), limiting the fluid–fluid interaction surface-area, and the inability to flow liquids through the channels. In this work a scalable synthesis route of nanoparticle stabilized fluid-bicontinuous gels with channels sizes below 500 nm and specific surface areas of 2 m^2 cm^{-3} is introduced. Moreover, it is demonstrated that liquids can be pumped through the fluid-bicontinuous gels via electroosmosis. The fast liquid flow in the fluid-bicontinuous gel facilitates their use for molecular separations in continuous-flow liquid–liquid extraction. Together with the high surface areas, liquid flow through fluid-bicontinuous gels enhances their potential as highly permeable porous materials with possible uses as micro-reaction media, fuel-cell components, and separation membranes.

1. Introduction

Nanostructured materials formed via the kinetic arrest of non-equilibrium self-assembly processes are an active field of research due to their rich diversity and the complexity of their formation pathways.[1–4] Fluid-bicontinuous gels are kinetically arrested colloidal gels that facilitate intimate contact between two immiscible liquids, while each liquid remains fully interconnected.[5,6] Recently, these structures have been employed for the fabrication of separation membranes,[7] microreactors,[8] sensors,[9] energy-storage devices,[10] carbon monoliths,[11] microropes,[12] and tissue engineering scaffolds.[13] However, limited control over their history dependent formation process and the inability to flow liquids through them has restricted their potentials until now.

Fluid-bicontinuous gels are obtained via the self-assembly of colloids on the interface of two interwoven liquids, such as oil and water. The assembly is driven by the reduction of the interfacial energy because the colloids remove contact area between the immiscible liquids. As a result, a close-packed colloidal monolayer is formed, which arrests the interwoven fluid arrangement mechanically to generate a bicontinuous interfacially jammed emulsion gel (bijel). The main pathway to obtain the bicontinuous fluid arrangement in a bijel is phase separation via spinodal decomposition.[14] Most frequently, spinodal decomposition is initiated by changing the temperature of a solution of two partially miscible liquids containing dispersed colloids.[6,9,11] However, the interfacial tension between fluids undergoing thermally-induced spinodal decomposition is not high enough to be able to employ nanoparticles (<100 nm) as interfacial stabilizers because their interfacial binding energy is too low. Instead, larger colloidal particles (>200 nm) are needed, resulting in fluid-bicontinuous gels with micrometer-sized fluid domains (>5 µm).[6,15] Sub-micrometer domains are crucial for the utilization of bijels in applications because of the larger surface area provided for mass transfer between the two liquids. In recent work, bijels with sub-micrometer domains have been obtained via vigorous agitation of emulsions together with nanoparticles and surfactants.[16] However, this method follows a batch fabrication protocol. Solvent transfer induced phase separation (STrIPS) enables both the use of nanoparticle stabilizers, as well as a continuous and scalable production route for bijels.[17,18] Prior to this work, STrIPS has only formed irregular bijels with sub-micrometer pores on the surface and micron-scaled, internal domains.[18,19] The high surface area achieved with sub-micrometer domains makes bijels ideal candidates to become mass transfer devices, where molecular exchange between the two liquids can take place through the interstitial spaces between the nanoparticles. Nevertheless, mass transfer in the bijel over hundreds of micrometers is limited by diffusion. To overcome this limitation, the seminal publication of the first conception of bijels in 2005 postulated that alternatively liquids could be actively pumped through the pore channel network; a prediction that, until now, remained to be experimentally realized.[5,20]

M. A. Khan, A. J. Sprockel, K. A. Macmillan, M. T. Alting, M. F. Haase
Van't Hoff Laboratory for Physical and Colloid Chemistry
Department of Chemistry
Debye Institute of Nanomaterials Science
Utrecht University
Utrecht 3584 CH, The Netherlands
E-mail: m.f.haase@uu.nl
S. P. Kharal, S. Boakye-Ansah
Department of Chemical Engineering
Rowan University
Glassboro, NJ 08028, USA
The ORCID identification number(s) for the author(s) of this article can be found under https://doi.org/10.1002/adma.202109547.

DOI: 10.1002/adma.202109547

Here, we present the successful production of bijels with internal sub-micrometer domains of the smallest pore sizes yet reported via a continuous and scalable synthesis method based on STrIPS and the realization of fluid flow through these bijels. In this work, we show that the non-equilibrium self-assembly process of nanoparticles during spinodal decomposition can be fully controlled. This control enables the formation of bijels with pores of 300–500 nm. The results from confocal microscopy, interfacial tensiometry, electron microscopy, and computer simulations are combined to give a complete discussion of the stabilization mechanisms of bijels with sub-micrometer-scaled features. With features this small, we find that the bijels have surface areas between the immiscible fluids of up to 2 m^2 cm^{-3}. After the detailed discussion of the formation of sub-micrometer domain bijels, we show that fluids can be flown through these bijels via electroosmosis over distances of several centimeters. This long overdue experimental demonstration paves the way for bijels to become media for continuous process microreactions. Here, we exhibit this potential on the example of continuous-flow liquid–liquid extraction in the bijel. Combining the small pore dimensions with fluid flow facilitates the use of bijels as highly permeable, fluid-bicontinuous gels with the potential to increase the efficiency of processes in catalysis,[21] membrane separations,[22] and energy-storage/conversion devices.[23]

2. Fabrication of Nanostructured Fluid-Bicontinuous Gels

The STrIPS process involves using two immiscible liquids, such as oil and water, that with the addition of a third solvent, such as alcohol, can become miscible. The volumes needed for mixing are given in the white region above the binodal curve in the ternary phase diagram of **Figure 1**a (Figure S1, Supporting Information). Once mixed, the removal of the solvent induces phase separation, often via the formation of water-in-oil or oil-in-water droplets (schematically depicted by black and magenta circles under the binodal curve in Figure 1a). In contrast, below the critical point (marked in green in Figure 1a), phase separation proceeds via the formation of interwoven oil and water channels (spinodal decomposition).[24] Unfortunately, this unique fluid arrangement is short lived because of the associated high interfacial energy. At last, two completely separated phases are formed by coarsening, minimizing the interfacial area between water and oil (Figure 1b-i). Fortunately, the phase separating interwoven fluid arrangement can be stabilized via self-assembly of colloidal particles on the oil/water interface, forming a kinetically arrested soft material named "bijel."[5,20] In a bijel, a rigid and percolating interfacial film of particles holds the interwoven fluids in place mechanically (Figure 1b-ii).

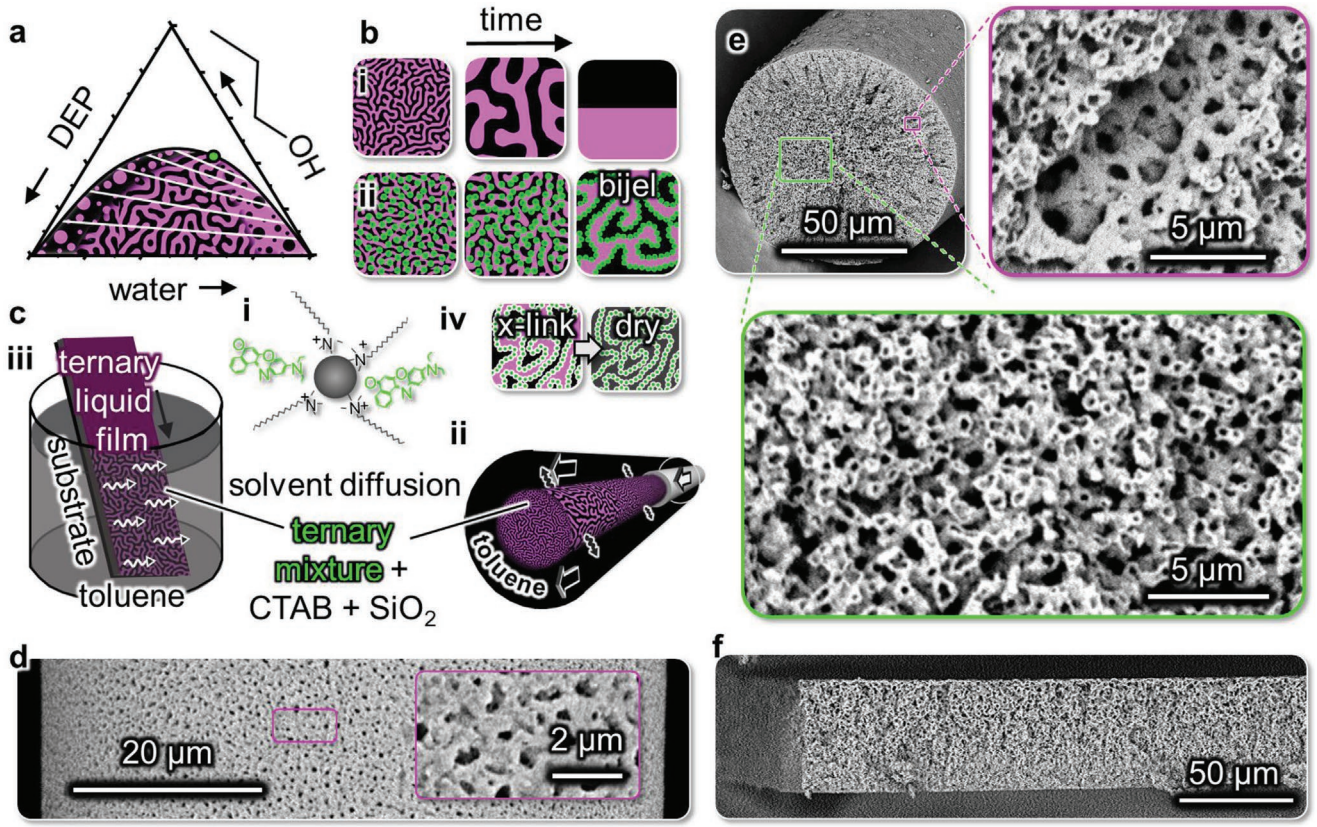

Figure 1. Bijel fiber and film synthesis. a) Ternary phase diagram plotting the miscible and immiscible regions in dependence of the volume fractions ϕ_i of water, diethyl phthalate (DEP) and 1-propanol (Figure S1, Supporting Information), the critical point is located at $\phi_{DEP} = 0.08$, $\phi_{1prop} = 0.42$, $\phi_{water} = 0.50$. b-i) Phase separation via spinodal decomposition of oil (black) and water (magenta); b-ii) bijel stabilization with nanoparticles (green). c-i) Particle modification with CTA^+ and Nile Red; c-ii) fiber formation; c-iii) film formation; c-iv) cross-linking with TEOS and drying; d) SEM image of fiber surface; (e) and (f) SEM images of percolating silica scaffold within the fiber and freestanding film, respectively (Figure S4, Supporting Information).

A stable bijel requires the particles to be equally wetted by both fluids. To this end, we employ silica nanoparticles (20 nm diameter, Ludox TMA) and tune their wettability in situ via the physisorption of cetyltrimethylammonium cations (CTA^+, Figure 1c-i).[25,26] A commercially available dispersion of Ludox TMA particles is dialyzed at a pH value of 3 and a NaCl concentration of 50 mmol L^{-1}. Next, a homogeneous dispersion of the particles and CTA^+ is prepared in a critical ternary mixture of water, diethyl phthalate (DEP), and 1-propanol. Interwoven fluids are formed in the mixture upon removal of 1-propanol via diffusion, a process termed STrIPS.[17] In the following, STrIPS is initiated either by flowing the mixture through an octadecyl trichlorosilane coated glass capillary into toluene (Figure 1c-ii) or by submerging an untreated glass slide coated with a thin film of the mixture into toluene (Figure 1c-iii). This results in the formation of semi-solid bijel fibers or films with yield stresses of 4–6 kPa (see Figure S2, Supporting Information).[27] The suitable CTA^+ concentration to obtain the interwoven fluid arrangement varies among different batches of the commercial grade Ludox TMA and typically ranges from 21 to 26 mmol per liter of the ternary liquid mixture. It can be determined rapidly by confocal microscopy analysis of fibers generated via pipetting the ternary liquid mixture into toluene (Figure S3, Supporting Information).

The fibers and films can be rigidified upon replacing the toluene with a solution of tetraethyl orthosilicate (TEOS) in light mineral oil after bijel formation. As was shown previously, TEOS cross-links the nanoparticles by producing additional silica at the particle surfaces,[8] enabling drying and visualization of the material with a scanning electron microscope (Figure 1d–f). Scanning electron microscopy (SEM analysis shows that the surface pores on fibers and films are connected to the oil filled channels of the interwoven fluid beneath the surface (Figure 1e and Figure S4, Supporting Information). A vast network of 300–500 nm sized oil channels is interwoven with 500–1000 nm sized water channels, an arrangement topologically analogous to a "plumber's nightmare."[28] Near the surface of the fiber, radially aligned and water filled macrovoids with sizes of several micrometers are observed. The same fluid arrangement can also be obtained in films generated with the ternary liquid mixture shown in Figure 1f. The unprecedented small oil channel sizes indicate that the coarsening of the interwoven fluids has been arrested at an early stage of the phase separation (Figure 1b-ii). Which factors enable the stabilization of sub-micrometer fluid channels here? In the following, we discuss how the stabilization is facilitated by the interfacial tension of the phase separating ternary mixture.

The driving force for nanoparticles to self-assemble on an interface is their interfacial attachment energy $\Delta E_{wo} = -\gamma_{wo}\pi r^2$, with γ_{wo} the water/oil interfacial tension, and r the radius of the spherical particle with a three-phase contact angle $\theta = 90°$.[29,30] This simplified formula does not take into account effects arising from line tension k (important for particles <10 nm, when k ranges from 10^{-11} to 10^{-9} N), which can change θ and result in adsorption barriers for particles.[31] To effectively stabilize a bijel, ΔE_{wo} must reach several hundred times the thermal energy kT of the particles, because this enables them to support the lateral stresses within the jammed interfacial nanoparticle film. After complete removal of propanol, the toluene/water interface reaches $\gamma_{wo} = 32$ mN m^{-1} (see Figure S5, Supporting Information). This results in a value for $\Delta E_{wo} = -2443\ kT$ for the 20 nm particles employed here, confirming sufficiently strong particle attachment for a stable bijel. In contrast, the most frequently used fluid mixture for thermally induced phase separation (TIPS), lutidine and water, reaches only $\gamma_{wo} = 0.6$ mN m^{-1} at a temperature needed for a stable bijel (60 °C).[32] For 20 nm particles, ΔE_{wo} calculates to $-46\ kT$, insufficient for a stable bijel. This explains why STrIPS facilitates the use of nanoparticles to stabilize the interwoven fluids, enabling submicrometer channel sizes, while thermally induced phase separation (TIPS) requires larger colloidal particles, thereby limiting the smallest possible channel dimensions.[6,11,15]

Why did previous studies on STrIPS not introduce the formation of sub-micrometer sized channels throughout the entire bijel structure?[17] Here, we can reproduce the structure of a typical STrIPS bijel by employing 2-propanol as the solvent. The 2-propanol bijel is shown in the confocal laser scanning microscopy z-stack in **Figure 2**a-i. Near the surface of the fiber (z = 5 µm) the nanoparticle stabilized interwoven oil/water channels have sizes ranging from 0.4 to 0.6 µm, while the center is composed of channels as big as 30 µm. In contrast, for the bijel formed with 1-propanol the pores in the center are as small as the surface pores of the 2-propanol bijel (Figure 2a-ii). To understand this difference, we analyze the mass transfer dynamics during STrIPS as well as their effect on the liquid–liquid interface and the nanoparticles for 1- and 2-propanol.

During STrIPS, propanol diffuses out and toluene diffuses into the ternary mixture as schematically depicted in Figure 2b. The mass transfer near the surface of the fiber is faster compared to the center due to the shorter diffusion distance and steeper propanol concentration gradient. As a result, the homogeneous ternary mixture phase separates radially inwards, forming toluene and water rich interwoven fluid channels over time. Eventually, pure water and toluene channels are obtained because both 1- and 2-propanol are infinitely diluted in the volumetrically larger toluene.

The time evolution of the liquid compositions during STrIPS is schematically depicted with curved arrows in the ternary phase diagrams in Figure 2c. Starting from the critical point, the volume fraction of propanol φ_{pr} decreases, crossing multiple tie-lines on its path to the horizontal axis with $\varphi_{pr} = 0$. The tie-lines have different slopes for 1- and 2-propanol (Figure 2c).[33] They are flat for 2-propanol, while for 1-propanol they are inclined near the critical point. Since the endpoints of the tie-lines give the compositions of the toluene and water rich phases, their slopes indicate the partitioning of 1- and 2-propanol. 2-propanol partitions equally between water and toluene. In contrast, 1-propanol partitions more into toluene. This partitioning behavior of 1-propanol is the main cause for the smaller bijel structures. The first important role the partitioning has is its influence on the time evolution of γ_{wo}, as discussed next.

Combining measurements of γ_{wo} with mass transfer simulations suggests that the interfacial activity of the nanoparticles increases faster with 1-propanol as compared to 2-propanol. To arrive at this conclusion, we model the non-equilibrium time evolution of γ_{wo} during STrIPS with equilibrium values of γ_{wo}. The validity of this approach is supported by the agreement of experiments with simulations described in Note S8, Supporting

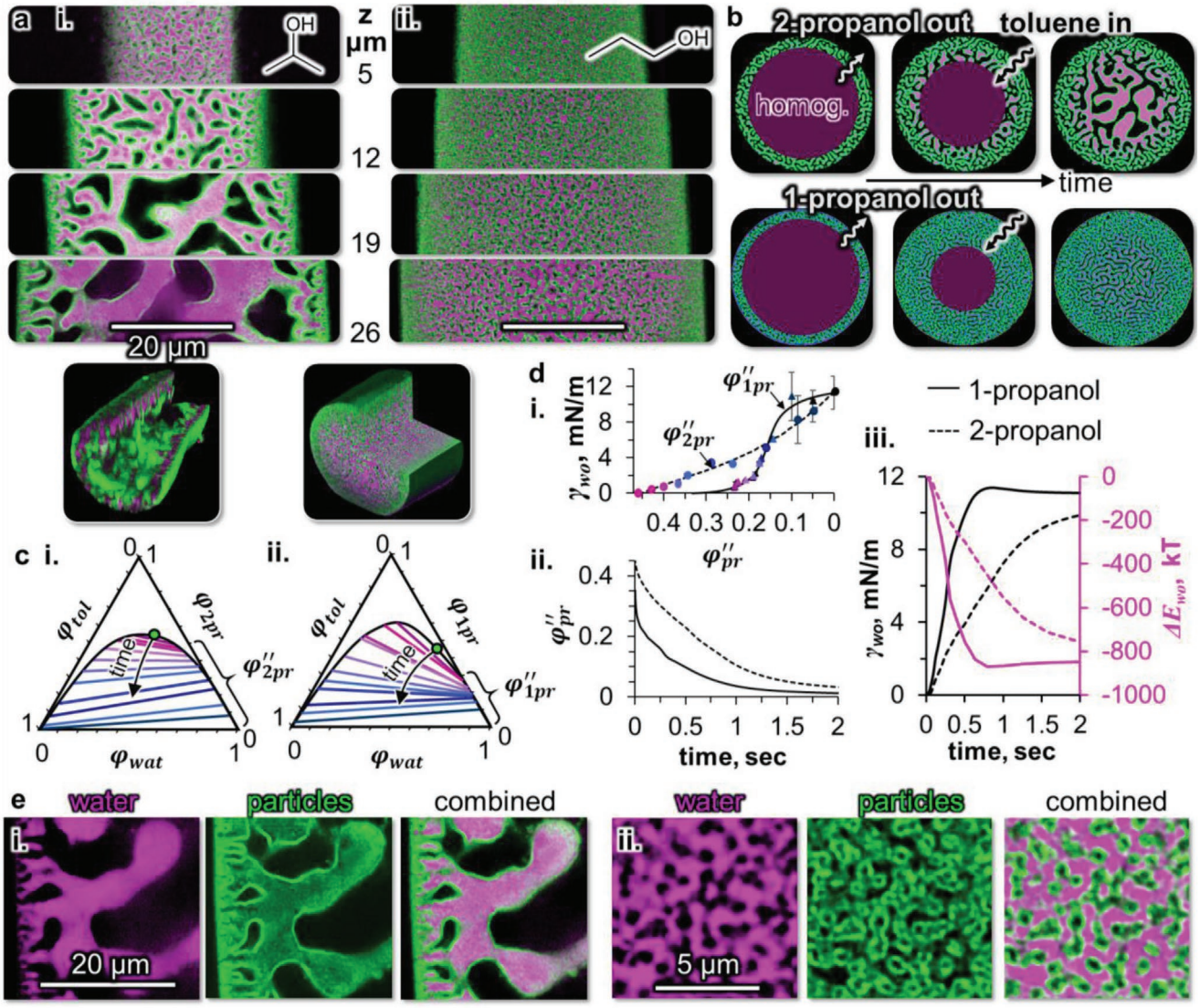

Figure 2. Interwoven fluids formed with 1- and 2-propanol. a) Confocal laser scanning microscopy images and their 3D reconstructions (bottom) of bijel fibers at different vertical distances from the surface (given as *z*-coordinate, Movie S1, Supporting Information). For sample preparation, the fibers are submerged in a solution of Nile red in n-hexane. Nile red diffuses into the bijel and adsorbs on the particles (see also Figure 1c-i). Upon blue laser light excitation (480 nm), adsorbed Nile red fluoresces in orange/red (550–700 nm), while Nile red dissolved in n-hexane fluoresces in green (500–550 nm, see Figure S10, Supporting Information). The fluorescence signal of the particles is false colored in green and the inverted fluorescence signal from n-hexane (water domains) is false colored in magenta. The water channels of the bijel include 30 vol% glycerol to enhance the optical transparency. From the confocal images we estimate the oil/water interfacial area of the 1-propanol bijel to reach 2 m^2 cm^{-3} (Figure S11, Supporting Information). b) Schematic depictions of the fiber cross section and the suggested structure formation dynamics during STrIPS for 1- and 2-propanol. c) Ternary phase diagrams (volume fraction φ based) for toluene and water with either 2-propanol (c-i) or 1-propanol (c-ii). d-i) Equilibrium interfacial tension between water rich ($''$) and toluene rich ($'$) phases in dependence of the propanol volume fractions in the water rich phase φ''_{1pr} and φ''_{2pr}; d-ii) diffusion simulation predicting average φ''_{1pr} and φ''_{2pr} within the fiber of 25 µm radius over time; d-iii) calculated values of the average interfacial tensions γ_{wo} and nanoparticle attachment energies ΔE_{wo} in the fiber over time. e) Confocal microscopy images of the different fluorescence channels of 2-propanol (e-i) and 1-propanol (e-ii) bijels.

Information. Figure 2d-i shows equilibrium measurements of γ_{wo} between toluene- and water-rich phases linked with a color code to the tie-lines of Figure 2c. Going downward in the ternary diagram (pink to blue tie-lines) results in an increase of γ_{wo}. The downward direction corresponds to a decreasing propanol volume fraction in the water rich phase φ''_{pr} (given by the right endpoint of the tie-lines in Figure 2c). The increase of γ_{wo} in Figure 2d-i has a higher slope for 1-propanol as compared to 2-propanol. We estimate the non-equilibrium γ_{wo} evolution during STrIPS by combining the trends in Figure 2d-i with a diffusion simulation predicting the average value of φ''_{pr} over time in the fiber (see Note S11, Supporting Information). The accuracy of the simulation has recently been supported by correctly predicting the density evolution of the phase separating liquid mixture.[34] Our simulation predicts that φ''_{pr} decreases faster for 1- as compared to 2-propanol (Figure 2d-ii).

High-speed video microscopy of phase separating droplets supports this prediction, showing experimentally that the phase separation with 1-propanol progresses faster than with 2-propanol (Figure S16, Supporting Information). From the simulated time dependence of φ''_{pr}, the time dependence of γ_{wo} is calculated. Figure 2d-iii shows that γ_{wo} increases faster with 1-propanol compared to 2-propanol. The faster increase of γ_{wo} indicates a higher interfacial activity of the nanoparticles at initial stages of STrIPS due to a quicker increase of the absolute value of $|\Delta E_{wo}|$. The expedited increase of $|\Delta E_{wo}|$ suggests that the interwoven fluids formed with 1-propanol can be stabilized earlier during STrIPS, providing a first possible explanation for the smaller fluid channels.

Before analyzing additional rationales for the fluid channel size dependence, we briefly discuss a limitation of our γ_{wo} measurements. The toluene- and water-rich phases used to measure γ_{wo} contain dissolved CTA^+ with concentrations representative of the ternary mixture employed to fabricate the bijels (Figure S5, Supporting Information). Because of the interfacial activity of CTA^+, the maximum value for $\gamma_{wo} = 11.5$ mN m^{-1} at $\varphi''_{pr} = 0$ (Figure 2d-i) is lower than for pure toluene/water (32 mN m^{-1}, Figure S5, Supporting Information). However, the adsorption of CTA^+ to the interface takes several seconds (see Figure S6, Supporting Information). Thus, the equilibrium values of γ_{wo} used in our analysis are lower than the nonequilibrium values of γ_{wo} during STrIPS. But, since the nonequilibrium dynamics of the CTA^+ adsorption affect STrIPS for both 1- and 2-propanol, our analysis still allows for a comparison between the two solvents. Nevertheless, more research is needed to fully understand the γ_{wo} evolution in the presence of CTA^+.

The partitioning of 1-propanol has a second important consequence for the bijel stabilization. It controls the partitioning of CTA^+ and the silica nanoparticles between the toluene- and water-rich phases during STrIPS. Confocal microscopy images in Figure 2e show that for both 1- and 2-propanol the nanoparticles have formed a fluorescent interfacial film. For 2-propanol there are also aggregated particles in the water phase (Figure 2e-i). In contrast, 1-propanol particles have aggregated in the toluene phase (Figure 2e-ii). Our measurements indicate that the presence of the CTA^+ modified particles in the toluene results from the strong partitioning of 1-propanol into this phase, which increases the CTA^+ solubility and therefore the particle dispersibility in toluene (Figure S17, Supporting Information).

The partitioning of CTA^+ to the toluene rich phase for 1-propanol results in contact angles θ of the particles close to 90° at CTA^+ concentrations used to make the bijel here. We determine this by measuring the emulsion type of vigorously agitated immiscible ternary mixtures with CTA^+ modified particles. Figure S18, Supporting Information, shows that for 1-propanol emulsion inversion from oil-in-water to water-in-oil occurs between 21–25 mM CTA^+. In contrast, for 2-propanol oil-in-water emulsions are formed for all CTA^+ concentrations. This suggests that $\theta \approx 90°$ for 1-propanol, while $\theta < 90°$ for 2-propanol during STrIPS. With the near neutral particle wettability with 1-propanol, the particles do not impose a curvature on the liquid–liquid interface. As a result, both positive and negative interfacial curvatures of the spinodally demixing oil/water channel network can be stabilized, resulting in the characteristic bijel structure throughout the entire fiber (Figure 2a-ii).

Last, the distinct particle partitioning also suggests different aggregation mechanisms. In the water phase, strong aggregation of the particles can occur due to the hydrophobic effect, as the CTA^+ covered particles disrupt the hydrogen bonding network of water.[35,36] Weaker particle aggregation driven by van der Waals interactions occurs in the toluene phase due to the lack of inter-particle repulsion.[37] The strong particle aggregation in water with 2-propanol as the solvent can limit the availability of individual particles for interfacial stabilization. Thus, the oil/water interface can coarsen for a longer period before interfacial jamming occurs. In contrast, the weaker aggregation in toluene with 1-propanol allows the particles to self-assemble more readily at the toluene/water interface, generating a robust interfacial film at early stages of the spinodal phase separation.

Concluding this section, STrIPS with 1-propanol generates nanostructured bijels because of the preferential partitioning of 1-propanol to the toluene-rich phase. The 1-propanol partitioning has 2 consequences: i) it facilitates a faster increase of $|\Delta E_{wo}|$, enabling more rapid bijel stabilization by the nanoparticles; and ii) it causes the CTA^+ and the nanoparticles to partition to the toluene-rich phase, resulting in particle contact angles close to 90° and enhanced colloidal stability during STrIPS.

3. Fluid Flow in Bijels via Electroosmosis

Next, we show that water can be pumped through the fibers after controlled alignment and chemical treatment. Pumping liquids through the fibers is important because it enables the fast transport of reactants in and out the bijel. In comparison, transport via diffusion is too slow to provide meaningful throughputs. Here, we employ electroosmosis as the pumping mechanism, since it enables the flow of water through the sub-micrometer channels without the application of high pressures that can damage the bijel structure. Electroosmosis is the bulk fluid transport in a channel, caused by the hydrodynamic drag from the electrophoretic movement of counterions of the channel wall.[38,39] In the bijel, the counterions are in the diffuse electric double layer of the percolating silica film. They can move in the direction of an externally applied electric field. Faster electroosmotic flow velocities are facilitated by higher silica surface charge densities due to the additional counterions.[40] To increase the surface charge, the bijels are submerged in a solution of triethylamine (TEA) in mineral oil. TEA partitions into the water channels, raises the pH value and deprotonates the Si–OH groups on the silica. We visualize the pH change in the bijel with the pH sensitive dye fluorescein (FITC). Confocal microscopy shows that the fluorescence of FITC in the water channels of the bijel becomes 4–5 fold stronger upon TEA introduction, confirming the pH increase (**Figure 3**a and Figure S19, Supporting Information).[41]

To pump water through the bijels, hundreds of parallel fiber segments are printed next to each other, TEOS hardened, and subsequently treated with TEA (Figure S20 and Movie S2, Supporting Information). At the cut-open ends of the fibers, water droplets are placed into which copper electrodes are submerged. Application of a voltage moves the water through the fibers from the positive to the negative electrode due to the

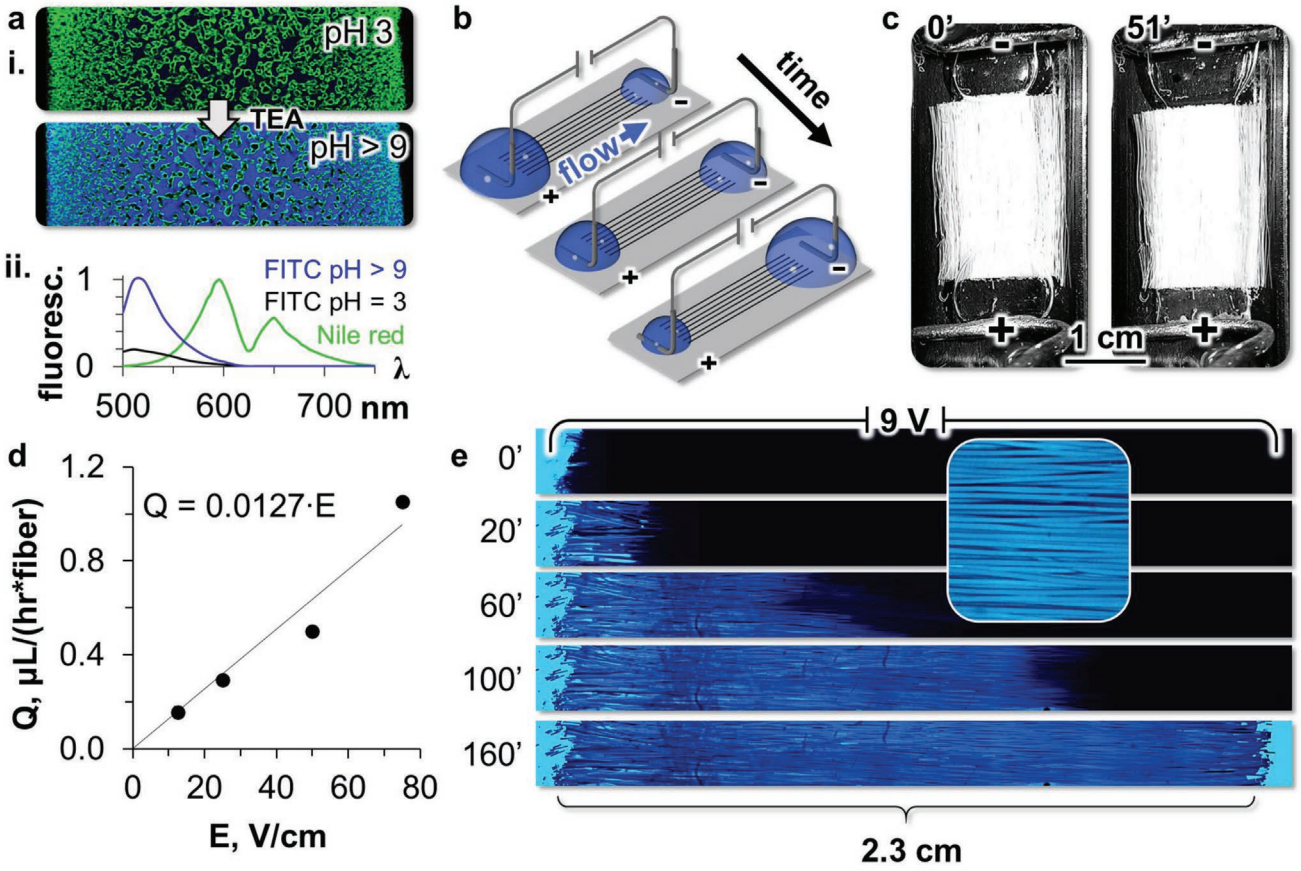

Figure 3. Advective flow in bijel fibers via electroosmosis. a-i) Confocal microscopy images of a bijel fiber segment before (pH 3) and after TEA introduction (pH > 9). The appearance of the blue (false) color results from the increased fluorescence of FITC at alkaline pH values. Green originates from Nile Red, adsorbed on the particles. a-ii) Fluorescence emission spectra of FITC before/after TEA introduction and adsorbed Nile Red. b) Schematic of electroosmotic flow experiment with water droplets at the end of the fibers. c) Photographs of water droplets and fibers before/after electroosmosis at a voltage of 100 V (Movie S3, Supporting Information). d) Volumetric flow rate through fibers in dependence of applied voltage. e) Confocal microscopy time series of the transport of 40 kDa PEG–FITC across the length of the fibers from one water droplet to the other (Movie S4, Supporting Information).

movement of the cationic counterions in the bijel (Figure 3b,c and Movie S3, Supporting Information).

At 150 V, 1 L of water can be flown in 3 h over a distance of 2 cm, passing over an interfacial area of 50 m^2. To this end, 24 cm^3 of bijel fibers with 50 µm diameter need to be printed. Approximately 0.018% of the transported water will undergo electrolysis (see Note S17, Supporting Information). The transport of large volumes of water is possible because the flow rate through the fibers scales roughly linearly with the applied voltage (Figure 3d). This linear dependence is in agreement with electrokinetic theory (Figure S21, Supporting Information).[38] Slight deviations from linearity are likely related to changes in the zeta potential of the silica due to the washing out of CTA^+. The silica scaffold remains fully intact after several hours of electroosmosis (Figure S22, Supporting Information). Electroosmosis also enables the transport of large polymeric solutes across the length of the bijel fibers. We show this here using polymer dye poly(ethylene glycol)–fluorescein isothiourea (PEG–FITC) with an average molar mass of 40 kDa (Figure 3e). At a voltage of 9 V, PEG–FITC has been transported from one end of the fiber to the other within 160 min (Movie S4, Supporting Information). It takes roughly 4 months to cover the same distance via diffusion of the polymer ($R_G \approx 9$ nm, $D \approx 2.4 \times 10^{-11}$ s^{-1}, Figure S23, Supporting Information).

4. Liquid–Liquid Extraction during Electroosmosis

To demonstrate potential uses of electroosmosis in the bijel, we introduce the application of continuous-flow extraction. As an example, the phase transfer of ethanol from oil to water is investigated. To this end, electroosmotic flow of water in the bijel is combined with pump driven flow of oil around the fibers. We design a crossflow device to stream oil with dissolved ethanol over the fibers (**Figure 4**a and Figures S24–S26, Supporting Information). A solution of 2 wt% ethanol in dodecane is flown in and out of the device by means of two syringe pumps. During the flow, ethanol is extracted from dodecane to water within the bijels. Simultaneously, electroosmotic flow transports the extracted ethanol towards the water reservoir with the negatively charged electrode (Figure 4a,b).

Increasing the voltage increases the extraction rate (Figure 4c). After 1 h of combined pump and electroosmotic driven flows, the ethanol amounts in both water reservoirs

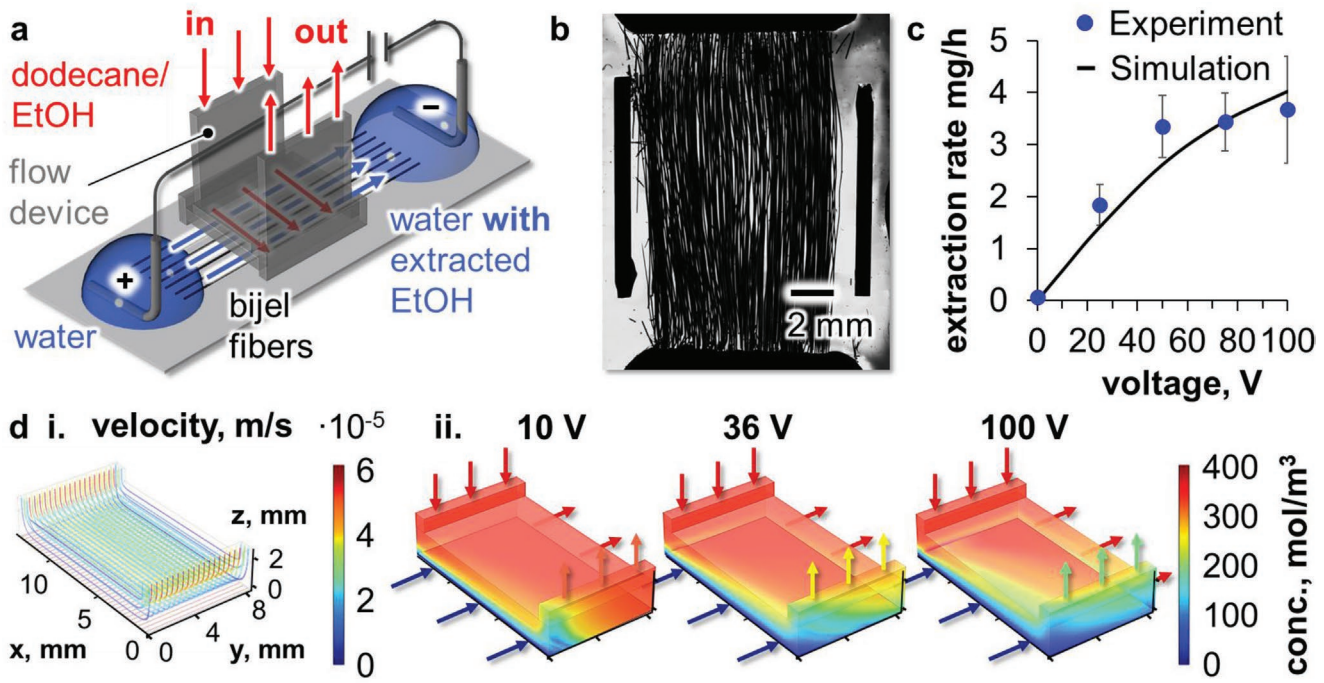

Figure 4. Continuous liquid–liquid extraction of ethanol to the bijel fibers. a) Schematic depiction of the experimental setup employed to flow a solution of ethanol in dodecane over the bijel fibers during electroosmosis. b) Overview microscopy image of fibers below flow device. c) Measured and simulated extraction rates of ethanol (EtOH) from dodecane to water for different applied voltages (dodecane flow rate 1 mL h^{-1} with 2 wt% ethanol, 600 × 50 µm diameter fibers, error bars correspond to the standard deviations of three experiments). d-i) Simulated velocity streamlines in dodecane; d-ii) calculated ethanol concentrations in dodecane above the fibers from a coupled flow/diffusion simulation (dodecane flow rate 1 mL h^{-1}, 2 wt% ethanol, water flow rates 0.038 mL h^{-1} (10 V), 0.137 mL h^{-1} (36 V), 0.381 mL h^{-1} (100 V) through fibers, Figure S25, Supporting Information).

are measured by gas chromatography (Figures S27–S29, Supporting Information). In the reservoir with the positive electrode the ethanol amount is negligible in all experiments. In contrast, the ethanol contents in the water reservoirs with the negative electrode increase with the voltage (divided by the experiment time in Figure 4c). Our finding shows that electroosmosis transports the ethanol through the fibers, and that the extraction rate can be controlled with the electroosmotic flow rate.

Numerical simulations can reproduce the measured extraction rates in dependence of the applied voltage (Figure 4d). In the simulation, the fibers are modelled as a continuous rectangular box below the dodecane flow. Water flows at the rates given in Figure 3d through this box. Both, the flow of dodecane and water are modelled with computational fluid dynamics (Figure 4d-i). The transport of ethanol is simulated via coupled flow and diffusion. Figure 4d-ii gives ethanol concentration distributions as surface plots for voltages ranging from 10–100 V. The simulations show how the concentration decreases toward the bottom (*z*-direction), as well as in both flow directions (*x*-, *y*-directions). At higher voltages (higher water flow through the bijel fibers), the ethanol concentration decreases stronger in the volume above the fibers. From these calculations the extraction rate is obtained and plotted in Figure 4c together with the measured values. Both experiment and simulation agree reasonably well, supporting the picture of combined flow and ethanol diffusion as the mechanism behind the extraction. These findings demonstrate the potentials for continuous-flow liquid–liquid extraction with bijel fibers. In future studies we plan to investigate the fascinating transport phenomena occurring during extraction to the bijel in more detail.

5. Conclusion

We have shown how bijels with sub-micrometer, interwoven fluid channels can be synthesized via STrIPS. The unprecedented small bijel channel sizes are facilitated by combining nanoparticles with immiscible liquids of high interfacial tensions (γ_{wo}). The solvent partitioning enables fast stabilization of the fluid-bicontinuous gels due to the rapid increase of γ_{wo}, the moderated nanoparticle aggregation, and the particle wetting modification by a cationic surfactant. The diffusion of molecules into the bijel and their phase transfer from oil to water are demonstrated. Water is pumped for the first time through the interwoven fluid channels via electroosmosis. Continuous-flow liquid–liquid extraction in bijels is introduced by combining electroosmosis with pump driven flow. These combined modes of transport have strong potentials for continuously operated phase transfer catalysis in bijels, an application with implications for sustainable chemical technologies.[21,42] Future research can introduce additional post-processing steps for the nanostructured bijels to become high surface area cross-flow reactors,[5] separation membranes for nanofiltration,[22] and biphasic transport components in fuel cells.[43]

Supporting Information

Supporting Information is available from the Wiley Online Library or from the author.

Acknowledgements

M.A.K. and A.J.S. contributed equally to this work. This project has received funding from the European Research Council (ERC) under the European Union's Horizon 2020 research and innovation programme (Grant agreement no. 802636). The authors thank Dominique Thies-Weesie for technical support and Jan Groenewold for insightful discussions.

Conflict of Interest

The authors declare no conflict of interest.

Data Availability Statement

The data that support the findings of this study are available from the corresponding author upon reasonable request.

Keywords

bijels, catalysis, electroosmosis, extraction, nanoparticles

Received: November 23, 2021
Revised: March 4, 2022
Published online: March 30, 2022

[1] R. Freeman, M. Han, Z. Álvarez, J. A. Lewis, J. R. Wester, N. Stephanopoulos, M. T. McClendon, C. Lynsky, J. M. Godbe, H. Sangji, *Science* **2018**, *362*, 808.
[2] H. Tsurusawa, J. Russo, M. Leocmach, H. Tanaka, *Nat. Mater.* **2017**, *16*, 1022.
[3] M.-A. Moradi, E. D. Eren, M. Chiappini, S. Rzadkiewicz, M. Goudzwaard, M. M. van Rijt, A. D. Keizer, A. F. Routh, M. Dijkstra, G. de With, *Nat. Mater.* **2021**, *20*, 541.
[4] B. Ruzicka, E. Zaccarelli, L. Zulian, R. Angelini, M. Sztucki, A. Moussaïd, T. Narayanan, F. Sciortino, *Nat. Mater.* **2011**, *10*, 56.
[5] K. Stratford, R. Adhikari, I. Pagonabarraga, J.-C. Desplat, M. E. Cates, *Science* **2005**, *309*, 2198.
[6] E. M. Herzig, K. White, A. B. Schofield, W. C. Poon, P. S. Clegg, *Nat. Mater.* **2007**, *6*, 966.
[7] M. F. Haase, H. Jeon, N. Hough, J. H. Kim, K. J. Stebe, D. Lee, *Nat. Commun.* **2017**, *8*, 1234.
[8] G. Di Vitantonio, T. Wang, M. F. Haase, K. J. Stebe, D. Lee, *ACS Nano* **2019**, *13*, 26.
[9] M. N. Lee, A. Mohraz, *Adv. Mater.* **2010**, *22*, 4836.
[10] D. Cai, F. H. Richter, J. H. Thijssen, P. G. Bruce, P. S. Clegg, *Mater. Horiz.* **2018**, *5*, 499.
[11] M. A. Santiago Cordoba, J. S. Spendelow, A. N. G. Parra-Vasquez, L. A. Kuettner, P. M. Welch, C. E. Hamilton, J. A. Oertel, J. G. Duque, E. J. Meierdierks, T. A. Semelsberger, *Adv. Funct. Mater.* **2020**, *30*, 1908383.
[12] S. P. Kharal, R. P. Hesketh, M. F. Haase, *Adv. Funct. Mater.* **2020**, *30*, 2003555.
[13] T. J. Thorson, E. L. Botvinick, A. Mohraz, *ACS Biomater. Sci. Eng.* **2018**, *4*, 587.
[14] P. S. Clegg, *Bijels: Bicontinuous Particle-Stabilized Emulsions*, Vol. *10*, Royal Society of Chemistry, London, UK **2020**.
[15] J. W. Tavacoli, J. H. Thijssen, A. B. Schofield, P. S. Clegg, *Adv. Funct. Mater.* **2011**, *21*, 2020.
[16] C. Huang, J. Forth, W. Wang, K. Hong, G. S. Smith, B. A. Helms, T. P. Russell, *Nat. Nanotechnol.* **2017**, *12*, 1060.
[17] M. F. Haase, K. J. Stebe, D. Lee, *Adv. Mater.* **2015**, *27*, 7065.
[18] S. Boakye-Ansah, M. S. Schwenger, M. F. Haase, *Soft Matter* **2019**, *15*, 3379.
[19] J. Li, H. Sun, M. Wang, *Langmuir* **2020**, *36*, 14644.
[20] M. E. Cates, P. S. Clegg, *Soft Matter* **2008**, *4*, 2132.
[21] S. Crossley, J. Faria, M. Shen, D. E. Resasco, *Science* **2010**, *327*, 68.
[22] S. Karan, Z. Jiang, A. G. Livingston, *Science* **2015**, *348*, 1347.
[23] S. J. Gross, K. M. McDevitt, D. R. Mumm, A. Mohraz, *ACS Appl. Mater. Interfaces* **2021**, *13*, 8528.
[24] A. J. Bray, *Adv. Phys.* **2002**, *51*, 481.
[25] B. P. Binks, J. A. Rodrigues, W. J. Frith, *Langmuir* **2007**, *23*, 3626.
[26] L. Tran, M. F. Haase, *Langmuir* **2019**, *35*, 8584.
[27] M. F. Haase, N. Sharifi-Mood, D. Lee, K. J. Stebe, *ACS Nano* **2016**, *10*, 6338.
[28] D. A. Huse, S. Leibler, *J. Phys. France* **1988**, *49*, 605.
[29] A. Koretsky, P. Kruglyakov, *Izv. Sib. Otd. Akad. Nauk USSR* **1971**, *2*, 139.
[30] B. P. Binks, T. S. Horozov, *Colloidal particles at liquid interfaces*, Cambridge University Press, Cambridge, UK **2006**.
[31] A. Stocco, M. Nobili, *Adv. Colloid Interface Sci.* **2017**, *247*, 223.
[32] C. A. Grattoni, R. A. Dawe, C. Y. Seah, J. D. Gray, *J. Chem. Eng. Data* **1993**, *38*, 516.
[33] A. Skrzecz, D. G. Shaw, A. Maczynski, A. Skrzecz, *J. Phys. Chem. Ref. Data* **1999**, *28*, 983.
[34] S. P. Kharal, M. F. Haase, *Small* **2022**, *18*, 2106826.
[35] D. Chandler, *Nature* **2005**, *437*, 640.
[36] S. Boakye-Ansah, M. A. Khan, M. F. Haase, *J. Phys. Chem. C* **2020**, *124*, 12417.
[37] M. Farrokhbin, B. Stojimirović, M. Galli, M. K. Aminian, Y. Hallez, G. Trefalt, *Phys. Chem. Chem. Phys.* **2019**, *21*, 18866.
[38] C. L. Rice, R. Whitehead, *J. Phys. Chem.* **1965**, *69*, 4017.
[39] S. Zeng, C.-H. Chen, J. C. Mikkelsen Jr, J. G. Santiago, *Sens. Actuators, B* **2001**, *79*, 107.
[40] L.-H. Yeh, S. Xue, S. W. Joo, S. Qian, J.-P. Hsu, *J. Phys. Chem. C* **2012**, *116*, 4209.
[41] E. Slyusareva, M. Gerasimov, A. Sizykh, L. Gornostaev, *Russ. Phys. J.* **2011**, *54*, 485.
[42] M. Pera-Titus, L. Leclercq, J. M. Clacens, F. De Campo, V. Nardello-Rataj, *Angew. Chem., Int. Ed.* **2015**, *54*, 2006.
[43] A. Forner-Cuenca, J. Biesdorf, L. Gubler, P. M. Kristiansen, T. J. Schmidt, P. Boillat, *Adv. Mater.* **2015**, *27*, 6317.